A facile approach to prepare a flexible sandwich-structured supercapacitor with rGO-coated cotton fabric as electrodes

Yuzhou Li, Yufan Zhang, Haoran Zhang, Tie-ling Xing [ID] * and Guo-qiang Chen

In recent years, the energy supply problem of wearable electronic equipment has become a topic of increasing concern. It is necessary to develop energy storage equipment with environmental protection, flexibility, a light quality and excellent performance. In this work, a solid, flexible and symmetrical supercapacitor based on graphene coated cotton fabric was fabricated. The flexible electrode materials were prepared through an environmentally friendly "dry-coating" method and subsequent "two step reduction" method of chemical and microwave reduction, the method is simple and convenient. The morphology and structure of prepared flexible electrode materials were characterized by scanning electron microscopy, X-ray diffraction, and Raman spectrometry. The supercapacitor was assembled in a sandwich structure and packaged and its electrochemical performance was investigated. The flexible sandwich structure (FSS) supercapacitor exhibits high capacitance (464 F g^{-1} at 0.25 A g^{-1}), good cycling stability (91.6% capacitance retention after 1000 charge and discharge cycles) and excellent electrochemical stability. This supercapacitor with easy fabrication, flexible and excellent electrochemical performance has potential to be used as a wearable device.

Introduction

In the last few decades, wearable electronics have been widely applied in information and communication, healthcare, fashion and military fields.[1]. The development trend of electronic fabrics drives the development of electronic devices and clothing technology.[2,3] Supercapacitors store energy by ion adsorption/desorption in the electrode/electrolyte interface or surface/near-surface reversible reactions.[4,5] Due to the ultrahigh power delivery, exceptional life cycle and efficiency, rapid charge and discharge capacities, a wide range of operation temperatures and adequate safety, supercapacitors are considered to be an extremely attractive alternative to rechargeable batteries.[6,7] Apparently, supercapacitor will even play a vital role in the future energy sustainable development.[5] Moreover, electroactive materials can be combined with textiles to form textile electrodes, which can be widely employed as flexible electrodes.[8,9]

Carbon materials have become the most widely used electrode materials in the field of supercapacitors because of their high specific surface area, good electrical conductivity, stable chemical properties, simple forming, low price, easy preparation and mature production technology.[10–12] Carbon materials have great potential as supercapacitor electrode materials due to their excellent mechanical properties and double layer

College of Textile and Clothing Engineering, Soochow University, Suzhou 215021, China. E-mail: xingtieling@suda.edu.cn; Tel: +86-512-6706-1175

capacitance properties. Researchers have made great efforts to construct supercapacitors using carbon-based materials, such as carbon nanotubes (CNTs),[13,14] activated carbon,[15] carbon fibers,[16] and graphene.[17–19] Compared with other carbon based materials, graphene has high specific surface area, high conductivity, high porosity and corrosion resistance, and is an ideal electrode material for energy storage devices.[20–22]

It is worth noting that supercapacitors could be fabricated on flexible substrates in a planar, all-solid-state structure.[23] So far, quite a number of materials including metal,[24] polymer,[25] silicone,[26] paper[27] and textile[28] have been used as substrates to construct flexible planar supercapacitors. Among them, textile should be the most attractive because of its extraordinary compatibility with conventional clothing industry.[29] Cotton fabrics have the advantages of low price, easy availability and good hydrophilicity, and are good materials for making flexible electrodes. The hydroxyl groups are favorable for water adsorption and reaction with chemical reagents.[30] The good adaptability of cotton fabric gives us the required curl ability. The combination of cotton fabric and conductive material not only maintains the original physical properties of the fabric, but also provides a self supporting active material support.[31] Therefore, cotton fabrics are considered to be ideal materials for the manufacture of releasable electrodes.

In the past few years, many researchers have focused on designing and fabricating rGO-cotton flexible electrodes for supercapacitor. Liu *et al.*[32]. prepared a flexible and easily processed electrode *via* a simple "brush-coating and drying"

process using common cotton cloth as the platform and a stable graphene oxide (GO) suspension as the ink, which showed the specific capacitance of 81.7 F g^{-1} (two-electrode system) in aqueous electrolyte. Bian et al.[33–35] improved the performance of carbon cloth electrode by constructing hierarchically porous nitrogen-doped carbon nanofiber layers or assembling porous NiO nanowires on carbon cloth. Bian et al.[36,37] reported polyaniline/graphene/polyester textile electrode materials and nitrogen-doped porous carbon nanotubes/carbon fabric electrodes with excellent electrochemical properties. Zhu et al.[38] prepared PPy/LGS (polypyrrole/lignosulfonate) coated cotton fabric via in situ oxidation polymerization of pyrrole in aqueous electrolyte. The prepared sample can reach a high specific capacitance of 304 F g^{-1} at a current density of 0.1 A g^{-1}. Xu et al.[39] synthesized graphene/cotton composite fabrics via a facile "dipping and drying" process followed by a NaBH$_4$ reduction method, and the prepared capacitor had a specific capacitance of 40 F g^{-1}. However, these methods were time-consuming, complicated and low efficient. Hence, a simple method to improve the performance and specific capacitance was proposed in this paper.

Herein, a solid, flexible and symmetrical supercapacitor was fabricated based on graphene coated cotton fabric. The flexible electrode materials were prepared through an environmentally friendly "dry-coating" method and subsequent "two step reduction" method of chemical and microwave reduction. To explore its electrochemical performance, cyclic voltammetry (CV), electrochemical impedance spectroscopy (EIS), galvanostatic charge/discharge (GCD) and Ragone plot were conducted. The cycling stability was also investigated to demonstrate its practical potentials for perspective applications in smart textiles and wearable electronics.

Experimental

Materials and reagents

Cotton fabric (308 g m^{-2}, warp density: 45 threads per cm; weft density: 21 threads per cm) was supplied by Jiangsu Huajia Group Co. Ltd. Graphite flakes ($\sim$325 mesh) were purchased from Alfa Aesar Co., Ltd. Sulphuric acid (H$_2$SO$_4$, 95–98%), phosphoric acid (H$_3$PO$_4$, 85%), ethanol (C$_2$H$_5$OH, 99.7%) and hydrogen peroxide (H$_2$O$_2$, 30%) were purchased from Chinasun Specialty Products Co., Ltd. Potassium permanganate (KMnO$_4$) and L-ascorbic acid were provided by Sinopharm Chemical Reagent Co., Ltd. Poly vinyl alcohol (PVA) was obtained from Shanghai Aladdin Bio-Chem Technology Co., Ltd. All chemical regents were analytical grade (AR) and directly used without further purification.

Preparation of GO hydrosol

GO was synthesized from graphite flakes by the improved Hummer's method.[40] Under the condition of ice water bath, 9 : 1 mixture of concentrated H$_2$SO$_4$ and H$_3$PO$_4$ (315 : 35 ml) was added to the 1000 ml flask containing 7 g graphite powder A. 49 g KMnO$_4$ was added into the system in batches within 30 minutes. The reaction system was maintained at 0 °C for 1.5 h in ice water bath. Then the reaction system was heated to 50 °C

and quickly stirred for 8 h. Afterwards it was cooled to 0 °C in ice water bath, and then 600 ml deionized water and H$_2$O$_2$ (30%) were added to stop the oxidation process. When the mixture turned golden yellow, the addition of H$_2$O$_2$ can be stopped, indicating highly oxidized GO was prepared. After one day of settling, the product was washed continuously with 200 ml deionized water and 220 ml ethanol. For each wash, the product was centrifuged at 10 000 rpm for 6 min. The prepared GO was added to a moderate amount of water and transferred into a dialysis bag (molecular weight cutoff: 8000–14 000 Da), and the GO hydrosol was prepared through dialysis for 3 days in deionized water. The concentration of GO thus obtained can be increased to 20–25 mg ml^{-1}.

Preparation of rGO coated cotton fabric

The prepared GOhydrosol ($\sim$25 mg ml^{-1}) was coated on cotton fabric (30 cm × 20 cm) fixed in a sample holder. The thickness of the GO hydrosol coated on the fabric surface was determined by adjusting the distance between the fabric and the scraper with feeler gauge. GO hydrosol was then poured onto the outside of the scraper. After adjusting the speed of the scraper coating, the scraper was started and the GO hydrosol can be coated on the cotton fabric surface smoothly. The fabric was dried in an oven at 120 °C for 10 min, and the dried GO hydrosol on the surface of the fabric would be dehydrated and converted to GO sheets. Using the same procedure to finish the other side of the fabric, GO-coated cotton fabric was obtained. The GO-coated cotton fabric was immersed in L-ascorbic acid (0.25 mol L^{-1}) at 90 °C for 2 h to reduce the GO sheets. In this step, oxygen-containing functional groups such as carboxyl (–COOH) and hydroxyl (–OH) were removed from GO. After reduction, the obtained cotton fabric was washed with a large amount of deionized water to remove the residual reducing agent, and then dried at 80 °C for 30 min. Afterwards, the obtained cotton fabric was further reduced in a domestic microwave oven (800 W, high power), and the GO sheets with uniform expansion can be obtained in just a few seconds. It was difficult for graphene oxide with low reductivity to be reduced under microwave conditions, because when graphite was oxidized, the π–π conjugate system was destroyed, and the microwave absorption capacity was greatly reduced. Graphene had conjugated electrons and conductivity after initial chemical reduction. Desorption of oxidative functional groups can be achieved by microwave heating, and GO was further reduced. Finally, the rGO-coated cotton fabric was obtained through the above "two step reduction" method.

FSS supercapacitor fabrication

AFSS supercapacitor was assembled by separating two pieces of rGO-coated cotton fabric electrodes with a raw cotton fabric separator, H$_3$PO$_4$/PVA gel electrolyte was prepared by adding 3 g poly vinyl alcohol (PVA) and 3 g phosphoric acid (H$_3$PO$_4$) in 30 ml of deionized water and heating at 90 °C for 2 h under constant speed stirring until a homogeneous viscous solution formed. The transparent solution was obtained after cooling it to room temperature. Before assembly, the two electrodes and

the cotton separator were immersed in the H_3PO_4/PVA gel electrolyte for 10 min, then cured at room temperature over 4 h, and 2 copper sheets were covered on positive and negative electrodes, respectively. Finally, they were assembled together and encapsulated with Ecoflex, then dried at room temperature for 12 h to remove the excess water in the electrolyte, and the FSS supercapacitor was obtained.

Characterization methods

The FTIR spectra of the samples were measured using Nicolet 5700 Fourier transformation infrared spectrometer (Thermo Electron Corporation), the scanning range was 400–4000 cm^{-1} and the resolution was 4 cm^{-1}. The crystal structure of the samples were identified by X-ray diffraction (XRD) with Cu-K$_\alpha$ radiation (X'pert-Pro MRD, Philips, NL), Cu-Kα ($\lambda = 0.1542$ nm), equal voltage and equal current were 40 kV and 30 mA respectively. The Multimode 8 atomic force microscope (Bruker, Billerica, MA, USA) was used to test the Lamellar thickness of samples. The SEM images of samples were measured using Hitachi TM 3030 desktop scanning electron microscope (Hitachi Ltd., Tokyo, Japan) to observe the surface morphology of samples and the test voltage was maintained at 15 kV. The Raman spectra (500–3000 cm^{-1}) of the samples were measured using a Horiba Jobin Yvon HR800 Raman spectrometer equipped with 50× objective lens, the excitation wavelength was 532 nm, the attenuation power was 25%,

and the acquisition time was 5 times. All electrochemical tests were performed on RST5000 electrochemical work station (Riset-est Electronic Co., Ltd., China). The elongation and strength of cotton fabric were tested by 3365 INSTRON materials testing machine. The effective test length and width were 25 cm × 6 cm. The contact angle of cotton fabric was measured by Krüss DSA 100 Optical Contact Angle instrument (Germany). The flexibility of cotton fabric was assessed by the bending property using an automatic pure bending tester (KES-FB-AUTO).

Results and discussion

Morphology and structure of the GO hydrosol

The key steps of preparation of RGO-coated cotton electrodes are shown in Fig. 1a–c. After double-sided dry coating, the color of the cotton fabric changed from white to brown, indicating that the GO hydrosol was successfully deposited on the fabric surface. After two-step reduction, the color of the cotton fabric changed from brown to black, which proved that majority of GO were reduced to rGO, and the RGO-coated cotton electrodes were successfully prepared. Fig. 1d shows the sandwich structure of supercapacitor assembly. From top to bottom, they are encapsulation film, copper sheet, flexible electrode, separator, flexible electrode, copper sheet and encapsulation film. The encapsulation film was made of ecoflex, raw cotton fabric was selected as the separator, and the electrodes were prepared according to the
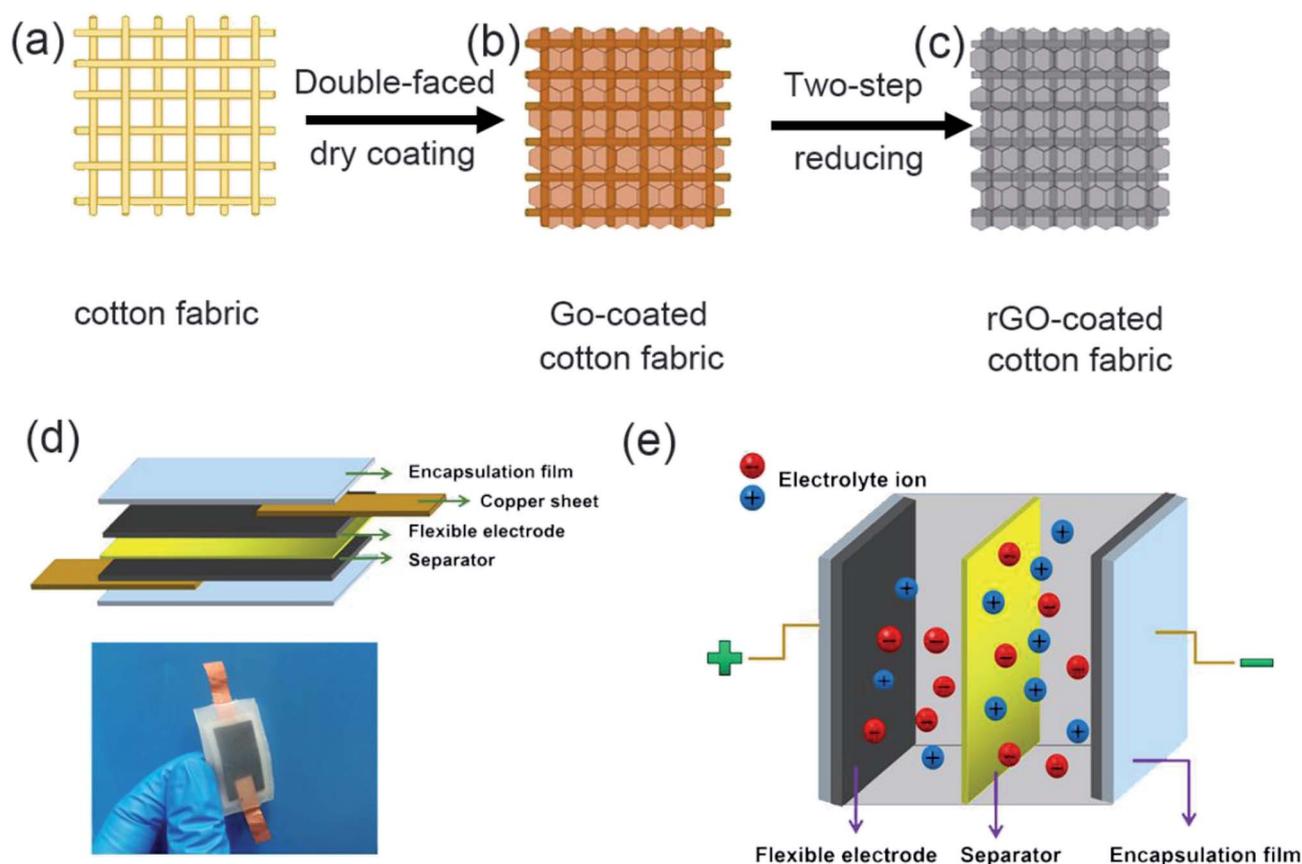

Fig. 1 Schematic illustration of the fabrication process of rGO-coated cotton fabric (a–c). Schematic diagram of sandwich structure supercapacitor assembly and the FSS supercapacitor device (d). Schematic diagram of the internal work of the FSS supercapacitor (e).

above method. The prepared electrodes and separator were soaked in the H_3PO_4/PVA gel electrolyte for 10 min, then assembled in accordance with the above assembly sequence, and a flexible supercapacitor, as shown in Fig. 1d, can be obtained. Fig. 1e shows the schematic diagram of the internal work of FSS supercapacitor. When the external electric field was applied to two electrodes, the electrolyte ions would migrate to the positive and negative poles under the action of the electric field and formed a double electric layer on the surface of the electrode. When the external electric field was removed, the positive and negative charges on the electrode and electrolyte ions with opposite charges attracted each other, resulting in a stable voltage difference between the positive and negative electrodes.[41]

FTIR, XRD and AFM spectra were utilized to characterize the structure of GO prepared in this work. In the FTIR spectra of GO (Fig. 2a), the absorption peaks at 3420 cm^{-1} and 1384 cm^{-1} correspond to the stretching vibration and the deformation vibration of the O–H respectively, while the C–H stretching vibration of the aldehyde corresponds to the 2920 cm^{-1} and 2852 cm^{-1}, and the absorption peak at 1617 cm^{-1} represents the skeleton vibration of the unoxidized graphite. In addition, the absorption peak at 1730 cm^{-1} is the characteristic band of C=O, and the absorption peak at 1110 cm^{-1} is attributed to the stretching vibration peak of C–O. The infrared spectrum of graphene oxide clearly reveals the successful transformation from graphite to GO. These oxygen rich functional groups enhance the activity of GO, which can improve the affinity with the fibers through chemical bonds. As shown in Fig. 2b, the strong and sharp characteristic diffraction peak of the flake graphite is found near 26.5°, corresponding to an interlayer spacing of 0.34 nm, indicating that the space arrangement of the flake graphite layer is very regular and has a good crystal
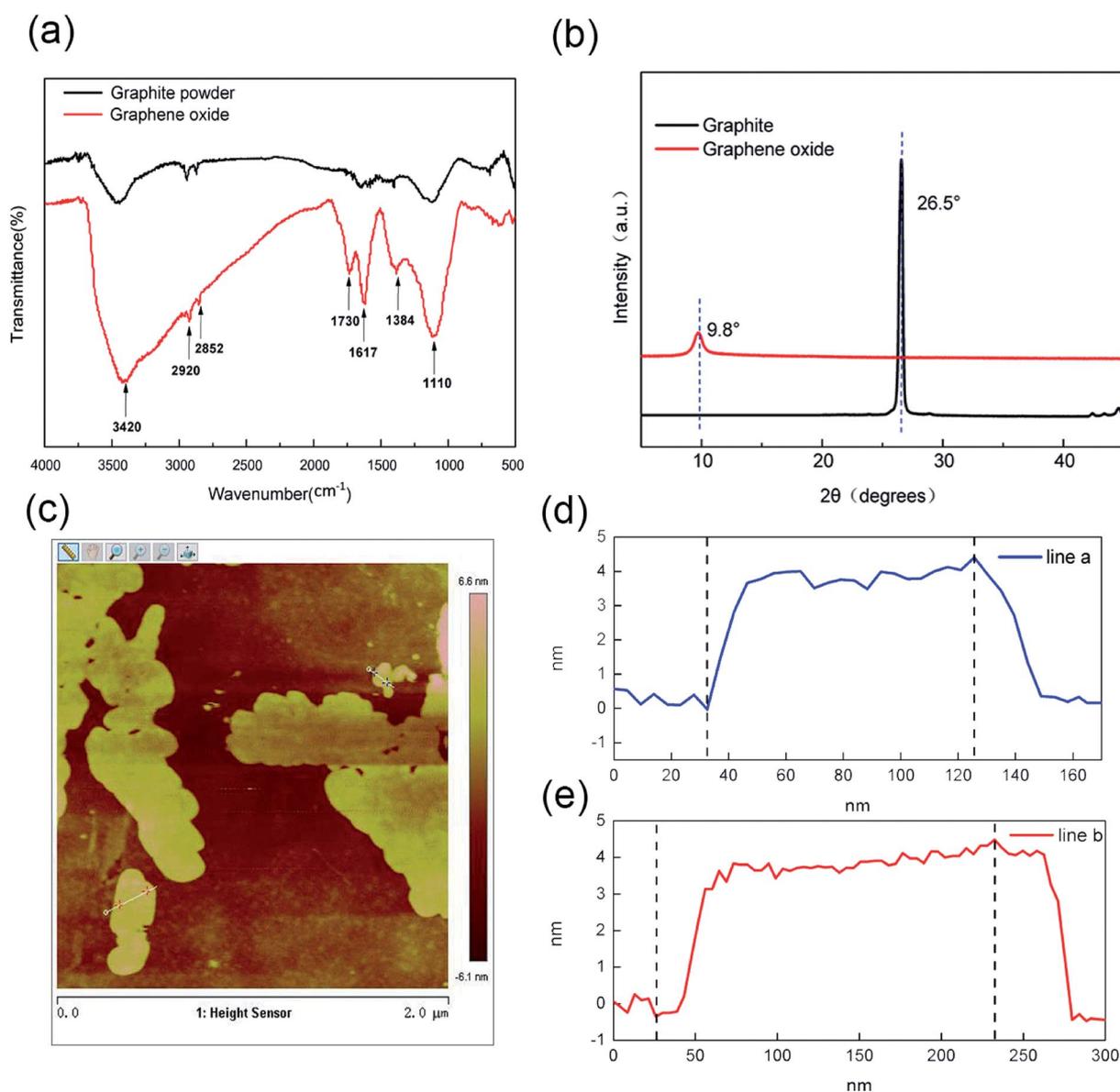

Fig. 2 FTIR spectra of graphite and graphene oxide (a). XRD spectra of graphite and graphene oxide (b). AFM images of GO sheets (c) and height profile of a single layer GO sheet (d and e).

structure. However, the characteristic peak of flake graphite disappears after the strong oxidation reaction, another wider and weaker characteristic peak appears at 10.8°. The interlayer spacing becomes larger because of the introduction of oxygen containing functional groups, indicating that the lamellar structure of the flake graphite is destroyed and a new crystal structure is formed. This result clearly demonstrated the successful transformation from graphite to GO. Fig. 2c shows the AFM image of GO, the sample used for AFM investigation was prepared by dropping the ultrasonic dispersion of GO suspensions onto the silicon wafer and vacuum drying at room temperature for 5 h. The cross-sectional images of two large and representative graphene oxide lamellae (Fig. 2d and e) show that the thickness of the lamellae is about 3–5 nm, and similar results have been observed by other AFM studies.[5,42]

Morphology and structure of the rGO-coated fabric

SEM was performed to characterize the morphologies of the pristine cotton fabric and the rGO-coated cotton fabric respectively. As shown in Fig. 3a and c, the images are the magnification of 100 and 1000 SEM images of pristine cotton fabric, respectively, while Fig. 3b and d are the magnification of 100 and 1000 SEM images of the rGO-coated cotton fabric, respectively. It can be seen from Fig. 3a and c that the pristine cotton fabric surface is smooth and clean, displaying a typically hierarchical pore network structure composed of micron-sized cotton fibers. The smooth surface provided a favourable

condition for the GO hydrosol to directly form GO sheets. As shown in Fig. 3b and d, a large amount of rGO sheets are located inside the spaces of cotton fibers, and the outer walls of the fibers are coated, the gaps between the fibers are also filled with rGO sheets, which confirms the deposition of graphene nanosheets on cotton fabric surface. The cross-sectional SEM image of rGO-coated cotton fabric can be observed from the insert. A layer of fibers on the surface of cotton fabric is coated with a large amount of rGO nanosheets, and the outer walls and interstices of the outer fibers are coated with rGO sheets. However, only a few of rGO nanosheets penetrate into the inner fibers, showing as inner cotton fibers and outer rGO nanofilm material.

XRD spectra was utilized to characterize the structure of cotton fabric coated with graphene, while Raman spectra was used to discuss the reduction change from GO-coated cotton fabric to rGO-coated cotton fabric. As shown in Fig. 4a, the characteristic bands in the Raman spectra of pristine cotton fabrics are disordered and irregular. However, in the Raman spectra of the cotton fabric coated with GO and rGO, there are only two obvious peaks at 1344 cm^{-1} and 1580 cm^{-1}, corresponding to the D band and G band, respectively. The G band in the Raman spectra of carbon nanomaterials represents the E_{2g} vibration model of the sp$_2$ carbon atom, indicating the ordered sp$_2$ bond structure, while the D band represents the defect and amorphous structure at the edge of the graphene. In addition, the intensity ratio of the G band to the D band also indicates the sp$_2$/sp$_3$ carbon ratio, which can characterize the reduction process of graphene oxide. The ratio of the D band to the G band
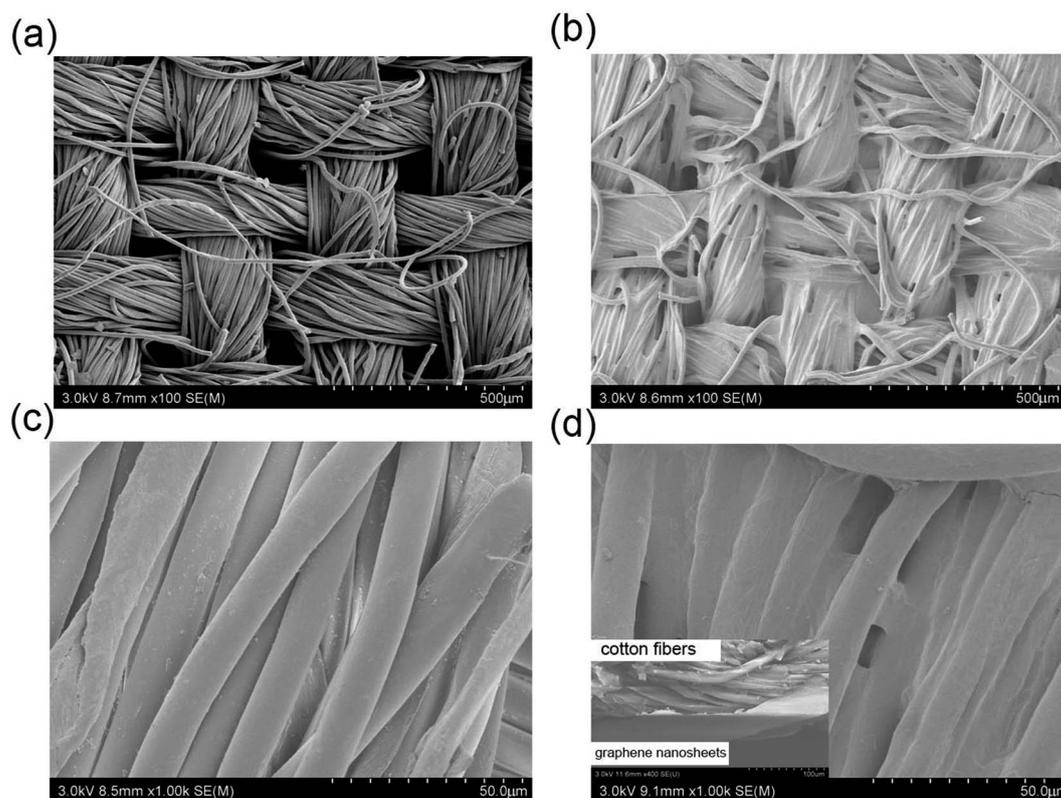

Fig. 3 SEM images of pristine cotton fabric (a & c), and SEM images of rGO-coated cotton fabric (b & d). With the cross-sectional SEM (inset).
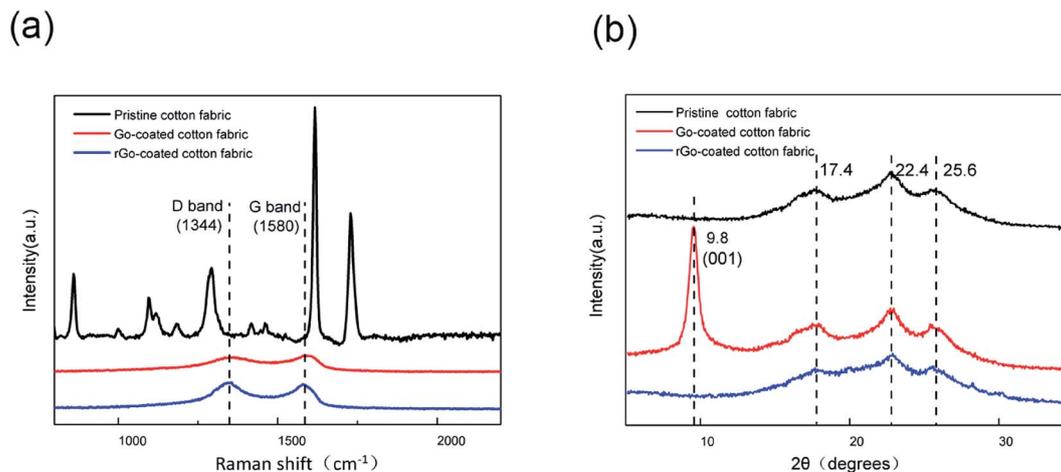
Fig. 4   Raman curves of pristine cotton fabric, GO-coated cotton fabric, and rGO-coated cotton fabric (a). XRD spectra of pristine cotton fabric, GO-coated cotton fabric, and rGO-coated cotton fabric (b).

of GO-coated cotton fabric was 0.91, and the ratio of the D band to the G band of rGO-coated cotton fabric increased to 1.06 after two-step reduction, demonstrating that the two-step reduction process removed the majority of oxygen rich functional groups in the GO, which further proved that GO was successfully reduced to graphene on the surface of cotton fabrics. It can be seen from Fig. 4b that the pristine cotton fabrics has 3 characteristic diffraction peaks at 17.4°, 22.4° and 25.6°. A new strong and sharp diffraction peak appears on the XRD spectrum of GO-coated cotton fabric at 9.8° corresponding to the (001) reflection, and the interlayer spacing becomes larger due to the introduction of oxygen containing functional groups on the graphite surface, indicating that GO has been successfully coated on the surface of the cotton fabric and combined firmly. After two-step reduction, it can be seen that the diffraction peak at 9.8° disappears, proving that the GO has been successfully reduced to graphene on the surface of cotton fabrics.

The hydrophobicity of pristine cotton fabric, GO-coated cotton fabric and rGO-coated cotton fabric were evaluated by Krüss DSA 100 Optical Contact Angle equipment (Germany). Fig. 5 shows water droplets on pristine cotton fabric, GO-coated cotton fabric and rGO-coated cotton fabric. As shown in Fig. 5a, the pristine cotton fabric can be easily wetted with water contact angle of 33.4° due to the abundant hydroxyl groups in its

structure. The contact angle of GO-coated cotton fabric is 61.8° (Fig. 5b), because GO nanoparticles are fully coated on the surface of cotton fibers, which prevents water from contacting the fibers surface. Additionally, the surface of GO coated cotton is rougher than that of pristine cotton. The contact angle of rGO coated fabric is 94.8° (Fig. 5c), and the rGO coated cotton fabric shows hydrophobicity to some extent. The phenomenon can be explained by the fact that rGO nanosheets covered interstices of cotton fibers, water penetrated into the fabric and decreased the air trap in cavities of fabric. Furthermore, intrinsic hydrophobicity and partial absence of polar functional groups of rGO was also responsible for the increase in hydrophobicity.

Electrochemical measurements

Fig. 6a shows the CV curves of the flexible sandwich structure (FSS) supercapacitor. It can be seen that the scanning voltage rate ascends from 20 mV s^{-1} to 160 mV s^{-1}, and the scanning potential windows are closed loops with good reversibility and are basically symmetric about zero current line, indicating fast charge transfer within the flexible electrode. There is no oxidation reduction peak on the CV curves and the curves have obvious rectangular characteristics under the smaller scanning voltage, indicating the efficient removal of the oxygen
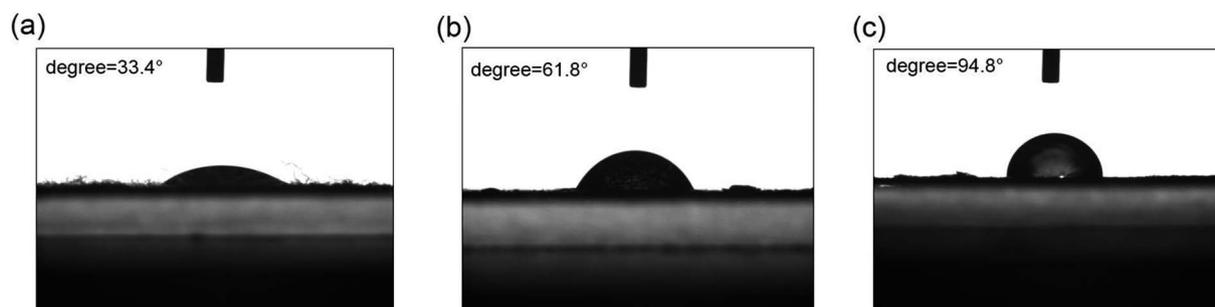

Fig. 5   The contact angles of pristine cotton fabric (a), GO-coated cotton fabric (b) and rGO-coated cotton fabric (c).
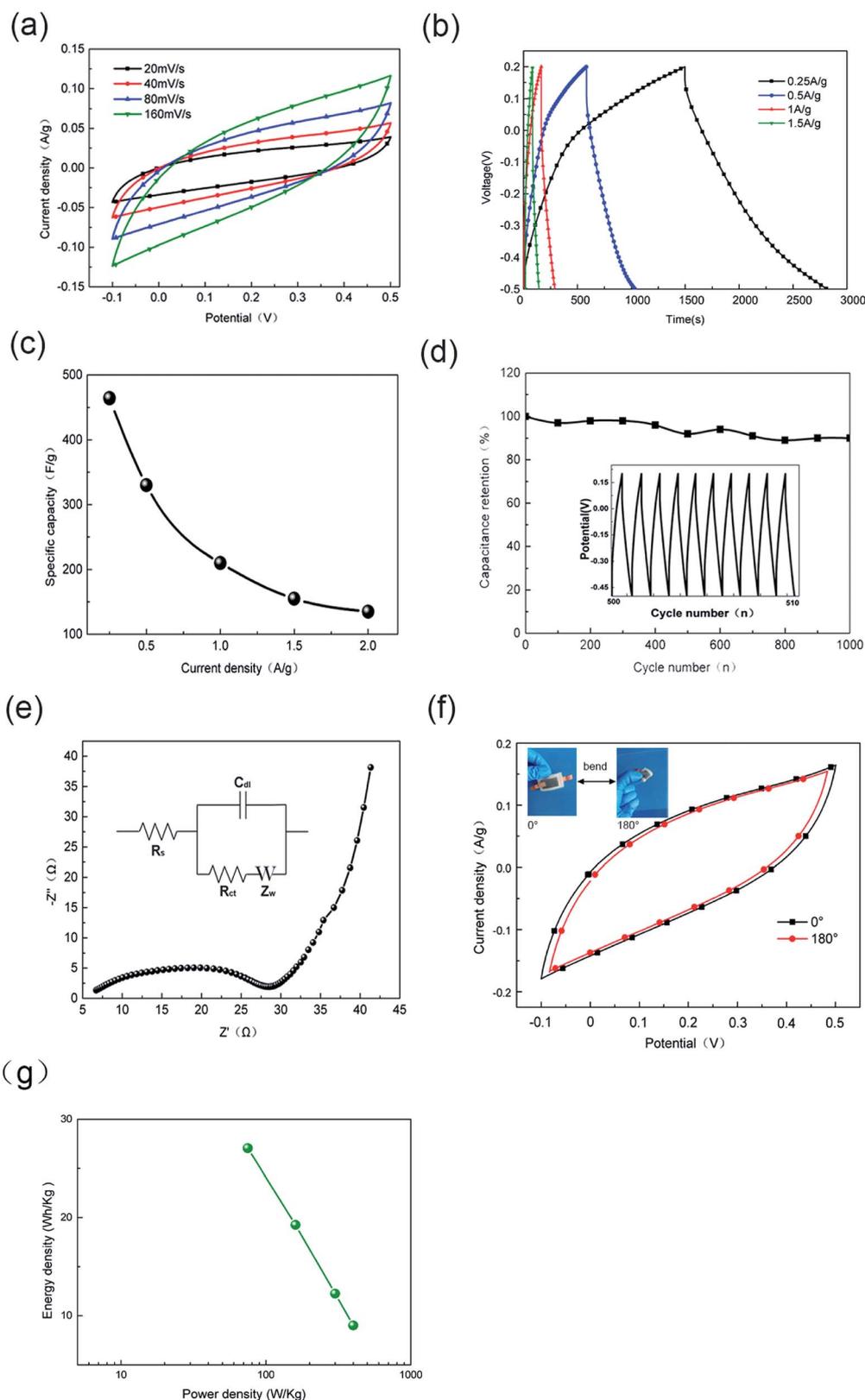
Fig. 6 CV curves of the asymmetric supercapacitor at different scan rates (a). Galvanostatic charge–discharge curves at different current densities (b). The calculated areal capacitance curve of the electrode according to the GCD curve (c). Capacitance retention of FSS super-capacitor during cycling tests, the inset shows the galvanostatic charge/discharge curve for the device (d). Nyquist plots for FSS supercapacitors (inset is the equivalent circuit diagram) (e). CV curves of the FSS supercapacitor under its flat and bending states (inset is the photograph of the FSS supercapacitor under flat and bending states) (f). Ragone plot relating energy density to power density of the FSS supercapacitors (g).

functional groups during reduction process. The capacity of the supercapacitor was almost entirely provided by the double layer capacitance and the contribution of pseudo capacitance was negligible. The GCD curves of the FSS supercapacitor at various current densities ranging from 0.25 to 1.5 A g^{-1} are shown in Fig. 6b. It can be seen that at different current densities, the voltage has a good linear relationship with time, indicating that there is no Faraday reaction on the surface of the electrode. Mainly the charge transfer reaction on the double layer. The curve is approximately isosceles triangle and does not change with the increase of the current density, further indicating that the capacity of the supercapacitor is almost entirely provided by the double layer capacitance with good reversibility, which is consistent with the CV curves. It can also be found that with the increase of the current density, there is no obvious voltage drop on the discharge curve, showing that the FSS supercapacitor has a good power characteristic. It may be attributed to the special pore structure of graphene, which contributes to the diffusion of electrolyte on the electrode surface. The specific capacitance of capacitors can be calculated according to eqn (1) and (2) [43,44] by galvano static charge/discharge test.

$$C = \frac{\Delta Q}{\Delta V} = \frac{I \Delta t}{\Delta V} \tag{1}$$

$$C_{\mathrm{m}} = \frac{C}{m} = \frac{I \Delta t}{m \Delta V} \tag{2}$$

I is charge/discharge current, Δt is discharge time, ΔV is discharge potential difference and m is the quality of active substances.

The change of specific capacitance of the FSS supercapacitor with current density is plotted in Fig. 6c. The quality of active substance is 0.002 g, with the increase of current density, the specific capacitance decreases and tends to be stable. The calculated specific capacitances are 464, 330, 210, 155, 135 F g^{-1} at various current densities of 0.25, 0.5, 1, 1.5, 2 A g^{-1}, respectively. These values are higher than the previous reported values.[32,38] Cyclic stability is an important indicator of the practical application of supercapacitor. The long-term cycling stability of the FSS supercapacitor was tested through a cyclic charge/discharge process at a fixed current density of 0.5 A g^{-1}. The result (Fig. 6d) shows that the specific capacitance decreases in the repeated testing process, but after repeated 1000 times, it can still maintain 91.6% of the original specific capacitance with less loss, indicating good electrochemical cyclic stability of FSS supercapacitor. The inset in Fig. 6d shows that the charging/discharging curves in the cycle remain triangular with no obvious change in shape. EIS is a very effective way to study the electrochemical performance of the supercapacitors.[5] Fig. 6e shows the Nyquist plot of the FSS supercapacitor. The high frequency area is semicircle, and the intersection point between the semicircle and the real axis is the electrode equivalent series resistance, and the intermediate frequency region is the diffusion area of the electrode material in the direction of the electrolyte ion. There is a certain angle between the low frequency and the real axis, showing that there is no "charge saturation" and partial capacitance of electrode

material has not been fully realized. The inset is the equivalent circuit of the supercapacitors, where R_{s} is solution resistance, C_{dl} is double layer capacitance, R_{ct} is interfacial charge transfer resistance, and Z_{w} is Warburg impedance of the ionic diffusion. Fig. 6f compares the CV curves of FSS supercapacitor at multiple states of $0°$ and $180°$. It can be seen that there is only a small gap between flat and bending state, indicating that the FSS supercapacitor has no apparent performance degradation and structural changes after bending.

It is an important to investigate the influence of coating on the elongation and tensile strength of fabrics. Table 1 shows that the elongation of pristine cotton fabrics is 21.92%, the elongation of rGO-coated cotton fabrics decreases to 15.39%. This was due to the reduction process reduced the toughness and elongation of rGO-coated cotton fabrics. The pristine cotton fabrics produce tensile strength mainly through the cohesive force between fibers. After rGO was coated on the surface of pristine cotton fabrics, the interfacial interaction improved the stress condition of the fabric, thus reducing the external force of the cotton fabrics and increasing the strength. The bending stiffness B of the fabric reflected the body of the fabric. The bending hysteresis moment 2HB indicates the fabric's elasticity and flexibility. B and 2HB of pristine cotton fabric and rGO-coated cotton fabric were tested by KES-FB-AUTO series testing instruments. Table 2 shows that the B and 2HB of rGO-coated cotton fabrics are 0.4743 gf cm^2 cm^{-1} and 0.7309 gf cm cm^{-1} respectively, indicating that rGO-coated cotton fabrics have certain flexibility.

Fig. 6g shows the relationship between energy density and power density of the FSS supercapacitors. Energy and power density are key parameters widely utilized to evaluate the property of energy storage device. Therefore, energy density and power density of the electrodes were calculated using the following eqn (3) and (4), where E_{m} and P_{m} represent the energy density and the power density, respectively. C_{m} represents the specific capacitance; ΔU is discharge potential difference and Δt is discharge time. The FSS supercapacitors possess a maximum energy density of 27.05 W h kg^{-1}. However, compared with

Table 1 The elongation and breaking strength of pristine cotton fabric and rGO-coated cotton fabric

	Elongation (%)	Breaking strength (N)
Pristine cotton fabric	21.92	581.34
rGO-coated cotton fabric	15.39	825.26

Table 2 The bending stiffness (B) and bending hysteresis moment (2HB) of pristine cotton fabric and rGO-coated cotton fabric

		B (gf cm^2 cm^{-1})	2HB (gf cm cm^{-1})
Pristine cotton fabric	Warp	0.1252	0.1137
	Weft	0.1235	0.1008
rGO-coated cotton fabric	Warp	0.4743	0.7309
	Weft	0.4472	0.7649

other reported flexible electrodes, its performance is higher than that of flexible and conductive nanocomposite electrode[32] and PPy/rGO[45]

$$E_{\mathrm{m}} = \frac{C_{\mathrm{m}} \Delta U^2}{2 \times 3.6} \tag{3}$$

$$P_{\mathrm{m}} = 3600 \times \frac{E_{\mathrm{m}}}{\Delta t} \tag{4}$$

Conclusions

In summary, a solid, flexible, symmetrical supercapacitor based on graphene coated cotton fabric was fabricated. The flexible electrode materials were prepared through an environmentally friendly "dry-coating" method and subsequently reduced with chemical and microwave "two step reduction" method. The FSS supercapacitor showed good capacitance performances and could be bent without obvious loss of capacitive performance, demonstrating the great potentials of flexible and foldable electrochemical capacitor for perspective applications in smart textiles and wearable electronics.

Conflicts of interest

There are no conflicts to declare.

Acknowledgements

References

1 C. Pang, C. Lee and K. Y. Suh, *J. Appl. Polym. Sci.*, 2013, **130**, 1429–1441.

2 Y. S. Su and A. Manthiram, *Nat. Commun.*, 2012, **3**, 1166.

3 R. Bao, C. Wang, L. Dong, R. Yu, K. Zhao, Z. L. Wang and C. Pan, *Adv. Funct. Mater.*, 2015, **25**, 2884–2891.

4 S. He and W. Chen, *J. Power Sources*, 2015, **294**, 150–158.

5 Q. Zhou, X. Ye, Z. Wan and C. Jia, *J. Power Sources*, 2015, **296**, 186–196.

6 L. Zhang, R. Zhou and X. Zhao, *J. Mater. Chem.*, 2010, **20**, 5983–5992.

7 Y. S. Wang, S. M. Li, S. T. Hsiao, W. Liao, P. H. Chen, S. Y. Yang, H. W. Tien, C. C. Ma and C. Hu, *Carbon*, 2014, **73**, 87–98.

8 K. Jost, C. R. Perez, J. K. Mcdonough, V. Presser, M. Heon, G. Dion and Y. Gogotsi, *Energy Environ. Sci.*, 2011, **4**, 5060–5067.

9 L. Hu, M. Pasta, F. L. Mantia, L. Cui, S. Jeong, H. D. Deshazer, J. W. Choi, S. M. Han and Y. Cui, *Nano Lett.*, 2010, **10**, 708–714.

10 X. Cao, Z. Yin and H. Zhang, *Energy Environ. Sci.*, 2014, **7**, 1850–1865.

11 U. N. Maiti, J. Lim, K. E. Lee, W. J. Lee and S. O. Kin, *Adv. Mater.*, 2014, **26**, 615–619.

12 N. Mahmood, C. Zhang, H. Yin and Y. Hou, *J. Mater. Chem. A*, 2013, **2**, 15–32.

13 M. Kaempgen, C. K. Chan, J. Ma, Y. Cui and G. Gruner, *Nano Lett.*, 2015, **9**, 1872–1876.

14 G. Wu, P. Tan, D. Wang, Z. Li, L. Peng, Y. Hu, C. Wang, W. Zhu, S. Chen and W. Chen, *Sci. Rep.*, 2017, **7**, 43676.

15 Y. Huang, Y. Liu, G. Zhao and J. Y. Chen, *J. Mater. Sci.*, 2017, **52**, 478–488.

16 Y. Huang, L. Peng, Y. Liu, G. Zhao, J. Y. Chen and G. Yu, *ACS Appl. Mater. Interfaces*, 2016, **8**, 15205–15215.

17 W. K. Chee, H. N. Lim, Z. Zainal, N. M. Huang, I. Harrison and Y. Andou, *J. Phys. Chem. C*, 2016, **120**, 4153–4172.

18 D. S. Sollami, A. D. Smith, J. Li and M. Östling, *Nanoscale*, 2017, **9**, 6998–7005.

19 Y. Jiang, X. Zheng, X. Yan, Y. Li, X. Zhao and Y. Zhang, *J. Colloid Interface Sci.*, 2017, **493**, 42–50.

20 Q. Wang, L. Jiao, H. Du, Y. Wang and H. Yuan, *J. Power Sources*, 2014, **245**, 101–106.

21 Z. F. Li, H. Zhang, Q. Liu, Y. Liu, L. Stanciu and J. Xie, *Carbon*, 2014, **71**, 257–267.

22 J. Hu, Z. Kang, F. Li and X. Huang, *Carbon*, 2014, **67**, 221–229.

23 L. Liu, Z. Niu and J. Chen, *Nano Res.*, 2017, **10**, 1524–1544.

24 L. Wang, Y. Han, X. Feng, J. Zhou, P. Qi and B. Wang, *Chem. Rev.*, 2016, **307**, 361–381.

25 M. Mastragostino, C. Arbizzani and F. Soavi, *J. Power Sources*, 2001, **97**, 812–815.

26 M. Areir, Y. Xu, D. Harrison and J. Fyson, *J. Mater. Sci.: Mater. Electron.*, 2017, **28**, 18254–18261.

27 S. L. Chou, J. Z. Wang, S. Y. Chew, H. K. Liu and S. X. Dou, *Electrochem. Commun.*, 2008, **10**, 1724–1727.

28 Y. Meng, Y. Zhao, C. Hu, H. Cheng, Y. Hu, Z. Zhang, G. Shi and L. Qu, *Adv. Mater.*, 2013, **25**, 2326–2331.

29 Z. Lu, C. Mao and H. Zhang, *J. Mater. Chem. C*, 2015, **3**, 4265–4268.

30 L. Allison, S. Hoxie and T. L. Andrew, *Chem. Commun.*, 2017, **53**, 7182–7193.

31 P. Ilanchezhiyan, A. S. Zakirov, G. M. Kumar, S. U. Yuldashev, H. D. Cho, T. W. Kang and A. T. Mamadalimov, *RSC Adv.*, 2015, **5**, 10697–10702.

32 W. Liu, X. Yan, J. Lang, C. Peng and Q. Xue, *J. Mater. Chem.*, 2012, **22**, 17245–17253.

33 Y. N. Liu, J. N. Zhang, H. T. Wang, X. H. Kang and S. W. Bian, *Mater. Chem. Front.*, 2019, **3**, 25–31.

34 Y. H. Peng, M. X. Guo, F. Shao, S. Liu, Q. Zhu and S. W. Bian, *RSC Adv.*, 2016, **6**, 74874–74877.

35 J. N. Zhang, P. Liu, C. Jin, L. N. Jin, S. W. Bian, Q. Zhu and B. Wang, *Electrochim. Acta*, 2017, **256**, 90–99.

36 Y. N. Liu, H. T. Wang, X. H. Kang, Y. F. Wang, S. Y. Yang and S. W. Bian, *J. Power Sources*, 2018, **402**, 413–421.

37 F. Shao, S. W. Bian, Q. Zhu, M. X. Guo, S. Liu and Y. H. Peng, *Chem.–Asian J.*, 2016, **11**, 1906–1912.

38 L. Zhu, L. Wu, Y. Sun, M. Li, J. Xu, Z. Bai, G. Liang, L. Liu, D. Fang and W. Xu, *RSC Adv.*, 2014, **4**, 6261–6266.

39 L. L. Xu, M. X. Guo, S. Liu and S. Bian, *RSC Adv.*, 2015, **5**, 25244–25249.

40 D. C. Marcano, D. V. Kosynkin, J. M. Berlin, A. Sinitskii, Z. Sun, A. Slesarev, L. B. Alemany, W. Lu and J. M. Tour, *ACS Nano*, 2010, **4**, 4806–4814.

41 E. G. Bushueva, P. S. Galkin, A. V. Okotrub, L. G. Bulusheva, N. N. Gavrilov, V. L. Kuznetsov and S. I. Moiseekov, *Phys. Status Solidi A*, 2010, **24**, 2296–2299.

42 F. Hauquier, D. Alamarguy, P. Viel, S. Noël, A. Filoramo, V. Huc, F. Houzé and S. Palacin, *Appl. Surf. Sci.*, 2012, **258**, 2920–2926.

43 P. Simon and Y. Gogotsi, *Nat. Mater.*, 2008, **7**, 845–854.

44 L. Zhao, L. Fan, M. Zhou, H. Guan, S. Qiao, M. Antonietti and M. M. Titirici, *Adv. Mater.*, 2010, **22**, 5202–5206.

45 J. Xu, D. Wang, Y. Yuan, W. Wei, L. Duan, L. Wang, H. Bao and W. Xu, *Org. Electron.*, 2015, **24**, 153–159.